CLINICAL AND
EXPERIMENTAL OPTOMETRY

Taylor & Francis
Taylor & Francis Group

Using clinical optical coherence tomography to characterise contact lens edge shape and base curve radius

Journal:	*Clinical and Experimental Optometry*
Manuscript ID	CEOptom-23-164-OP.R2
Manuscript Type:	Original Research Paper
Date Submitted by the Author:	18-Oct-2023
Complete List of Authors:	Mallada, Sofia; Universidad de Zaragoza, Applied Physics Yebra, Diana; Universidad de Zaragoza, Applied Physics Zardoya, Nerea; Universidad de Zaragoza, Applied Physics Garcia, JORGE; Universidad de Zaragoza, Applied Physics
Keywords:	contact lenses, OCT, contact lens edge, back optic zone radius

Abstract:	Clinical relevance: Clinical optical coherence tomography devices are widely used in optometry and ophthalmology and may be used to measure contact lens base curvature radius and visualise contact lens edge shape. Background: Knowledge of contact lens geometry facilitates fitting, while optical coherence tomography provides a powerful means of measuring geometrical form. This study evaluates the performance of a clinical optical coherence tomography device (3D OCT-1000) in characterising contact lens edge shape and measuring the back optic zone radius of rigid gas-permeable contact lenses in vitro. Methods: First, an opto-mechanical optical coherence tomography contact lens adaptor was designed and 3D-printed to facilitate a contact lens being imaged using a commercial optical coherence tomography device. Second, several image-processing algorithms and a simple calibration method were developed to measure back optic zone radius in optical coherence tomography B-scans. Finally, based on the findings of two experiments, B-scan performance was evaluated in terms of 1) capacity to differentiate between contact lens edge geometries, and 2) capacity to obtain accurate and repeatable back optic zone radius measurements. Statistical and graphical analyses were performed to characterise reliability and reproducibility. Results: The 3D OCT-1000 and adaptor combination was capable of acquiring images of sufficient quality to discriminate between soft and rigid contact lens edge geometries. Additionally, statistical analysis of the rigid contact lens measurements demonstrated satisfactory back optic zone radius measurement accuracy and reproducibility. Conclusion: This study demonstrates that a 3D OCT-1000 fitted with an opto-mechanical adaptor combination can be used to assess contact lens edges in vitro and that this clinical optical coherence tomography device, combined with image processing and linear calibration of the B-scans, is capable of obtaining back optic zone radius measurements of rigid gas-permeable contact lenses that are close to the ISO 18369-2:2018

	manufacturing tolerance range (±0.05 mm).

SCHOLARONE™
Manuscripts

CEOptom-23-164-OP

RESEARCH

Using clinical optical coherence tomography to characterise contact lens edge shape and base curve radius

Sofia Otin Mallada,[a] Diana Gargallo Yebra, [a] Nerea Tolón Zardoya, [a] Jorge Ares García [a]

Applied Physics, University of Zaragoza, Zaragoza, Spain

ARTICLE HISTORY

Received:

Revised:

Accepted:

KEY WORDS

back optic zone radius, contact lens edge, contact lenses, optical coherence tomography.

[Corresponding author]

Jorge Ares García**:** fatxutxa@unizar.es

Abstract

Clinical relevance: Clinical optical coherence tomography devices are widely used in optometry and ophthalmology and may be used to measure contact lens base curvature radius and visualise contact lens edge shape.

Background: Knowledge of contact lens geometry facilitates fitting, while optical coherence tomography provides a powerful means of measuring geometrical form. This study evaluates the performance of a clinical optical coherence tomography device (3D OCT-1000) in characterising contact lens edge shape and measuring the back optic zone radius of rigid gas-permeable contact lenses in vitro.

Methods: First, an opto-mechanical optical coherence tomography contact lens adaptor was designed and 3D-printed to facilitate a contact lens being imaged using a commercial optical coherence tomography device. Second, several image-processing algorithms and a simple calibration method were developed to measure back optic zone radius in optical coherence tomography B-scans. Finally, based on the findings of two experiments, B-scan performance was evaluated in terms of 1) capacity to differentiate between contact lens edge geometries, and 2) capacity to obtain accurate and repeatable back optic zone radius measurements. Statistical and graphical analyses were performed to characterise reliability and reproducibility.

Results: The 3D OCT-1000 and adaptor combination was capable of acquiring images of sufficient quality to discriminate between soft and rigid contact lens edge geometries. Additionally, statistical analysis of the rigid contact lens measurements demonstrated satisfactory back optic zone radius measurement accuracy and reproducibility.

Conclusion: This study demonstrates that a 3D OCT-1000 fitted with an opto-mechanical adaptor combination can be used to assess contact lens edges in vitro and that this clinical optical coherence tomography device, combined with image processing and linear calibration of the B-scans, is capable of obtaining back optic zone radius measurements of rigid gas-permeable contact lenses that are close to the ISO 18369-2:2018 manufacturing tolerance range (±0.05 mm).

[Introduction]

Optical coherence tomography (OCT) devices[1] are widely used in optometry and ophthalmology clinics to diagnose and study eye health[2,3] and/or to observe and evaluate contact lens fitting.[4,5,6] Alternatively, some researchers are also using the high-accuracy interferometric capabilities of OCT to measure the mechanical properties of soft contact lenses[7] and the geometric shape of eye surfaces *in vivo*.[8-12] Since OCT devices can achieve very accurate geometric measurements when used appropriately, several researchers have successfully demonstrated the application of specific lab-built spectral domain OCT devices in measuring the topographic surface and central thickness of intraocular lenses[13,14] and rigid and/or soft contact lenses *in vitro*,[15-17] achieving sufficient sensitivity to discriminate changes in soft contact lenses after use.[18,19]

Recently, an OCT device designed to measure contact and intraocular lenses achieved consistent results within the ISO 18369-3:2018[20] tolerance ranges for curvature radius and central thickness.[21,22] This technology could help practitioners monitor the geometry of contact lenses fitted in patients. For instance, it could assist in determining contact lens edge shape profile, which is difficult to assess non-destructively.[23,24] Unfortunately, OCT devices marketed for *in vivo* ocular examination cannot easily measure contact lenses *in vitro* for two main reasons: 1) device design does not permit proper positioning of the lenses, and 2) clinical OCT device manufacturers do not usually provide information about the spatial geometric transformations performed on B-scan data. Therefore, any spatial information recovered from B-scan data in a clinical OCT device should always be treated with caution.

In this study, a specific opto-mechanical adaptor was developed to measure contact lenses using an OCT device marketed for clinical application (Topcon 3D OCT-1000). In addition, a linear calibration model and image-processing methods were developed to retrieve accurate geometric measurements from B-scan data provided by this clinical OCT device.

Methods

Two experiments were conducted to test the ability of the OCT device to monitor contact lens geometry. In the first experiment, B-scans of the edges of various rigid and soft contact lenses were acquired with the OCT device and an opto-mechanical adaptor. The second experiment measured the back optic zone radius (BOZR) of a rigid contact lens sample. To achieve this, the posterior radius measurements of the device were calibrated against reference values obtained using an optical radiuscope. Next, repeatability between sessions and operators was tested.

Finally, statistical analysis was performed on two independent series of measurements taken in different sessions to compare the accuracy of the OCT measurements with those of the radiuscope.

Contact lenses

The edge assessment experiment employed a set of 8 soft and rigid contact lenses (corneal and scleral; see Table 1). The set was chosen as a representative sample of the contact lenses found at accessible research and teaching laboratories.

For the BOZR experiment, 18 monofocal (-3.00 D) rigid gas-permeable spherical contact lenses with a 6.00 mm optical zone diameter and central BOZRs from 7.30–8.40 mm were used. These lenses were manufactured by Lenticon Pharmaceutical SA (Madrid, Spain) from Polycon II copolymer (Silafocon A).

Instrumentation

A Neitz CG-X optical radiuscope (Sterling Ultra Precision, AMETEK, USA) was used to measure the vertex radii of curvature of the back surface of the contact lenses at a resolution of 0.01 mm.

OCT device and contact lens adaptor

A 3D OCT-1000 clinical spectral domain OCT device was used (Topcon Co.; central wavelength: 840 nm; bandwidth at half maximum: 50 nm). Maximum in-air axial resolution can therefore be estimated from the coherence length formula of the standard light source[1] for a Gaussian spectrum as $\Delta z = 2 \times \ln(2) / \pi \times \lambda_c^2 / \Delta\lambda_{FWHM} = 6.23\ \mu m$.[$\Delta z$ = maximum in-air axial resolution, λ_c = central wavelength, $\Delta\lambda_{FWHM}$ = bandwidth at half-maximum of the spectrum].

Maximum light exposure power at the corneal plane position was less than 0.65 mW and maximum lateral resolution was better than 20 µm. In anterior segment scanning mode, the device acquires B-scans with a lateral scanning range of 6 mm and an axial range of 2 mm. An opto-mechanical OCT contact lens adaptor was designed using Inventor® Software (AutoDesk Inc. USA) and fabricated from polylactic acid using a commercial fused deposition modelling printer. The adaptor included a movable holder for positioning a tilted flat mirror. This mirror was employed to redirect the probe beam toward the contact lens surface and to collect and redirect the backscattered beam toward the pupil entrance of the OCT device (Figure 1). In its current form, the adaptor is not designed to measure soft lenses immersed in saline solution. This capability can be achieved, however, using a cuvette with planar transparent walls.

B-scan to assess contact lens edge geometry

The contact lens adaptor was used to capture 6-mm-wide B-scans with the ability to perform transverse movements. Trained operators acquired and exported the B-scans as 1143 × 617 24-bit colour images. As the images were only taken to show the image quality that this clinical OCT device can achieve for edge lens geometry analysis, there was no attempt to locate the azimuthal meridian position of each sample.

Optical distortion caused by different curves and refractive indices or by distortion of the OCT cross-scan was not corrected since the edge B-scans were only for qualitative observation.

BOZR measurements using the optical radiuscope

The radiuscope, calibrated as per ISO 18369-3:2018,[20] served as the reference standard for measuring BOZR after confirming the surface regularity of the contact lenses using the above-mentioned surface microscope. A trained operator repeated 5 measurements on each lens to increase precision and the average was calculated. The contact lens was removed and reinserted into the holder before each measurement to simulate real measurement conditions.

B-Scan of the posterior curve of rigid contact lenses

The measurement procedure was as follows:

(1) The contact lens was placed on the OCT device contact lens adaptor in a stabilised horizontal position with the concave side facing up.

(2) The contact lens was transversely aligned with the optical axis of the OCT device.

(3) The axial position of the OCT device was adjusted to position the image profile within the reference axial interval on the B-scan live video display.

(4) 6-mm-wide horizontal B-scans were acquired in anterior chamber measurement mode and exported as portable network graphics files.

To research inter-session repeatability, Operator1 repeated the same measurements in a different session. Under this procedure, two data sets – Operator1-Session1 and Operator1-Session2 – were generated. To research inter-operator repeatability, Operator2 repeated the entire procedure for all contact lenses, obtaining an image set named Operator2-Session1.

BOZR calculation from B-scans

To estimate the BOZR from B-scans, image processing and curve fitting are required. A program was written (Matlab R2019b, Mathworks Inc) to perform the operations in the flow-chart shown in Figure 2. These operations included colour-to-intensity conversion, noise filtering to increase B-scan signal-to-noise ratio, automatic intensity thresholding to avoid background noise[25] and image segmentation to pre-process the exported B-scan data before analysis.

Once the region corresponding to the posterior curve was segmented, local centroid calculations[26] were performed to estimate, with subpixel precision, the axial position of each scattering point of the posterior curve of the contact lens. Finally, least squares were used to fit pairs of XZ centroid coordinates to a general circle profile to estimate the BOZR.[27]

Prior to conducting experiments, the curvature radius estimation algorithm was evaluated using noise-free synthetic B-scans. The results confirmed that the described procedure accurately estimates the curvature radius from noise-free synthetic B-scans of circle curves with nominal radii ranging from 7.30–8.40 mm. The absolute value of the maximum error and the standard deviation of the difference between the estimated radii and the nominal ones were 0.006 mm and 0.0013 mm, respectively.

Moreover, to estimate the limit of precision for curvature radius measurements due to spatial random noise, a simulation was conducted using the same set of synthetic concave coordinate profiles corrupted with additive Gaussian noise with a standard deviation of 6.23 µm. The simulation, for nominal curvature radii ranging from 7.30–8.40 mm, resulted in a maximum error of 0.065 mm and a standard deviation of the difference of 0.018 mm (i.e. an order of magnitude higher than in the noise-free case).

BOZR linear calibration from an initial measurement sample

As the processes before image export, scanning distortion and the reference refractive index are unknown for this clinical OCT device, simple linear calibration was performed using a set of radiuscope reference values. Starting with an initial pixel size of 5.25 µm, the radiuscope measurements were used to calculate the parameters (aa and bb) for a linear calibration function, which minimised the average squared error between the Operator1 and radiuscope measurements (optical radiuscope = aa × BOZRestimation + bb). The results of this process were aa = 0.695106, bb = 0.047948 mm and r-squared = 0.981469. The slope of the linear fit (aa) accounted for the pixel calibration and reference refractive index, while the z-intercept (bb) accounted for systematic errors caused by fan-scanning distortion.

Statistical analysis

To assess the precision and accuracy of the OCT BOZR measurements, statistical analyses were performed using IBM SPSS Statistics V.20. The absolute maximum differences between OCT and radiuscope BOZR measurements were evaluated along with the standard deviation of the difference. The variation coefficient was calculated for each sample as the ratio 100 × standard deviation of difference / <radiuscope BOZR measurements>, where <radiuscope BOZR measurements> is the average of the radiuscope BOZR values of the whole sample, providing a measure of the relative error of each measurement versus the reference values.

Normal data distribution was analysed using the Shapiro–Wilk test and parametric tests for contrast data analysis. Inter-observer and inter-session repeatability were assessed using *t*-tests for paired samples between measurements taken by different operators (BOZROperator1-Session1 vs BOZROperator2-Session1) and the same operator in two different sessions (BOZROperator1-Session1 vs BOZROperator1-Session2).

A p-value < 0.05 was considered statistically significant. Bland–Altman plots were used to explore systematic differences between measurements taken by different operators and sessions. The limits of agreement were calculated as the mean ±1.96 standard deviation.

Finally, to evaluate the accuracy of OCT-based BOZR measurements (BOZROperator1-Session1, BOZROperator2-Session1) versus the radiuscope, Student's *t*-test for paired samples and the intra-class correlation coefficient were used. Bland–Altman plots were also used to explore systematic differences between BOZR radiuscope and OCT-based measurements.

Results

B-scans of contact lens edges

Figure 3 shows B-scans (454 × 170 pixels) of contact lens edges that have been cropped and presented in 24-bit colour without additional image processing. The images were taken to demonstrate the ability to discriminate between different edge geometries (rigid gas-permeable contact lens edges (blue) and soft contact lens edges (red)). The same cropping and scaling sizes (see scale marking in Figure 3(f)) were used for all sub-images.

BOZR of a rigid gas-permeable contact lens set

One hundred sixty-two B-scan profiles were acquired and processed to estimate the BOZR for all the samples in the contact lens set. Table A (Appendix A) displays the mean and standard deviation of BOZR values obtained from processed B-scans (BOZROperator1-Session1, BOZROperator1-Session2, BOZROperator2-Session1) along with nominal BOZR and mean radiuscope BOZR measurements. BOZROperator1-Session1 represents the mean and standard deviation of BOZR values obtained from Operator1-Session1 measurements; BOZROperator1-Session2 corresponds to the mean and standard deviation of BOZR values estimated by

Operator1 during Session2; BOZROperator2-Session1 shows the mean and standard deviation of BOZR values estimated from Operator2 B-scans.

The top of Table 2 shows the standard deviation, maximum BOZR error and variation coefficient values versus the average values of the radiuscope BOZR measurements for each OCT measurement series. For the sake of completeness, the results equivalent to those described in the preliminary numerical simulations testing the image-processing algorithm are presented in the same table in dark red italic font. As can be seen, the BOZR measurements based on B-scan data show much higher standard deviations (standard deviation of the Operator1-Session1 difference = 0.059 mm, standard deviation of Operator1-Session2 difference = 0.039 mm, standard deviation of Operator2-Session1 difference = 0.059 mm) and maximum absolute errors (Operator1-Session1 = 0.110 mm, Operator1-Session2 = 0.104 mm, Operator2-Session1 = 0.130 mm) than those obtained in noise-free conditions (standard deviation of no noise difference = 0.0013 mm, maximum absolute error of no noise = 0.006 mm). They are also higher than the errors estimated by minimum spatial noise simulation (minimum = 0.018 mm, maximum = 0.065 mm).

The paired *t*-test results and the intra-class correlation coefficient analysis to assess intra-operator and intra-session repeatability are shown at the bottom of Table 2. The measurements taken by the OCT operators do not present significant statistical differences: p-value = 0.660 and p-value = 0.997 for BOZROperator1-Session1 vs BOZROperator2-Session1 and BOZROperator1-Session2 vs BOZROperator2-Session1, respectively. Moreover, testing BOZROperator1-Session1 vs BOZROperator1-Session2 resulted in p-value = 0.666, indicating that good intra-operator repeatability is achievable.

Finally, the results of comparison between BOZR with radiuscope and BOZR OCT-based measurements are also shown in Table 2, which shows Student's *t*-test results for BOZROperator1-Session1 vs radiuscope BOZR (p-value = 0.661), BOZROperator2-Session1 vs radiuscope BOZR (p-value = 0.996) and intra-class correlation coefficients between the radiuscope measurement and BOZR obtained for Operator1 (0.992($p < 0.001$)) and Operator2 (0.991($p < 0.001$)).

Bland–Altmann plot

Intra-session agreement is shown in Figure 4(a), while inter-observer agreement is illustrated in Figure 4(b). Mean difference is represented by a solid red line; dashed red lines show the 95% confidence intervals for the mean difference; grey-shaded regions indicate ISO 18369-2:2018 manufacturing tolerance limits (±0.05 mm)[28].

[Figure 4 near here].

The differences between radiuscope measurements and OCT-based measurements for two different operators in the sessions that were not used for the linear calibration (Operator1-Session1 and Operator2-Session1) are shown in Figure 5(a) and Figure 5(b).

Discussion

An opto-mechanical adaptor was created for clinical use and fitted to an OCT device to acquire B-scans of light scattering from contact lens surfaces. The system qualitatively assessed the edge geometry of different contact lens models and measured BOZRs of 3D spherical rigid gas-permeable contact lenses.

Qualitative assessment of edge geometry

The findings confirm the validity of using acquired B-scans to discriminate between the rounded edges of rigid gas-permeable contact lenses and the more peaked edges of soft contact lenses (Figure 3). This finding is significant because it provides a non-destructive way of differentiating between contact lens characteristics. OCT-based edge imaging has only previously been achieved using lab-built instruments[5,23,29,30] or by fitting contact lenses on real eyes,[31,32,33,34,35] making these results particularly noteworthy.

Figure 3(c,d) shows the greater peripheral thickness with which scleral lenses are manufactured versus other contact lenses. Consequently, as clearly shown, the slopes of both sides of the scleral contact lenses need to change quickly to form the edge of the lens. The acquired B-scans also enabled estimation of the depth of the engraving mark of a rigid gas-permeable torical contact lens (Figure 3(b)). This subtle finding suggests that the combination of the adapter and OCT could be used to monitor the damage that appears on the edges and surface of contact lenses due to use.

Finally, in the images in Figure 3, and unlike other studies using specific lab-built OCT devices,[36-38] optical geometrical distortion and refraction index path-length modulation were not corrected. Geometrical information extracted from these images must therefore be treated with caution.

BOZR measurements

Several researchers have successfully used lab-built OCT devices to measure the geometry of optical refractive surfaces from OCT B-scans and have noted that the key to success at this task differs between the first exposed surface and subsequent posterior surfaces. Measurement of surfaces placed after the refraction caused by preceding ones requires correction of the distortion inherent to the OCT transverse scan, knowledge of the preceding refractive indexes and surface geometries and application of an optimal estimation technique that efficiently uses all available information.[37-39] Conversely, measurement of the geometry of a first exposed surface only requires correction of the distortion due to transversal scanning or, alternatively, use of scanning methods that do not introduce geometrical distortions caused by non-telecentric lateral scanning.[13]

The lack of technical information about the spatial distortion correction algorithms used by the clinical OCT device led this study to explore the feasibility of employing straightforward linear calibration to obtain an accurate BOZR estimation from a spherical rigid contact lens sample. Using B-scans for BOZR measurement also meant developing image-processing algorithms capable of estimating the BOZR value for a rigid gas-permeable contact lens sample.

The results corroborate previous findings made with a prototype Optimec is830 device developed specifically for contact lens inspection;[23] there were no statistically significant differences between the OCT-based BOZR measurements and those measured by an optical radiuscope (see Table 2). Figure 5(a,b) shows that almost all OCT-based BOZR measurements (26/36) were within the ISO tolerance range. The repeatability findings are also consistent with those obtained by Huang et al.[13] when measuring an intraocular lens using a lab-built OCT device free of geometric scanning distortion, as well as with those obtained by Karnowski et al.[15] when measuring soft contact lenses using a spectral domain OCT device developed in-house. In both studies, BOZR measurement repeatability is in the order of 0.08 mm (0.065 mm for the Optimec is830, and an estimated 0.1085 mm for the 36 D intraocular lens, assuming an equiconvex geometry), similar to the 0.059 mm obtained for Operator1-Session1 and Operator1-Session2 in relation to the radiuscope measurements.

The fact that the experimental standard deviations for the OCT-based measurements triple the ones obtained by numerical simulation with minimum spatial random noise (0.018 mm) suggests that placing and removing the contact lenses for each measurement may constitute an additional noise input in BOZR measurement. To test this hypothesis, additional series of 30 consecutive BOZR measurements were performed on the three rigid contact lenses with nominal BOZR = [7.30, 7.80, 8.40] mm, keeping them in the same transversal position throughout the procedure. This latter experiment produced smaller standard deviations (0.023 mm, 0.035 mm, 0.028 mm) in each case.

It could therefore be argued that, due to image-processing artefacts, the system is not operating at the physical limit of axial resolution or that the spatial noise is higher than that calculated from the coherence length of the optical source of the OCT device[1]. It is nonetheless noteworthy that the precision achieved in this study is close to the physical limit. Additional research is needed to further understand and potentially improve system precision.

Bland–Altmann plots

Figure 5(a) shows a weak correlation between the difference in radiuscope reference values, Operator1 OCT measurements and average curvature radius. This trend is also visible in the intra-session repeatability shown in the Bland–Altmann plot (Figure 4(b)), indicating that linear calibration may be insufficient. However, this trend is not present in the Operator2 measurements (Figure 5(b)) or in the intra-observer Bland–Altmann plot (Figure 4(b)), indicating that a more complex calibration model may not be necessary. In fact, almost all the measurements are within the ISO 18369-2:2018 manufacturing tolerance range[28] (±0.05 mm) for rigid gas-permeable contact lenses. Nevertheless, the BOZR measurement reproducibility reported in this paper was generally worse than stipulated in ISO 18369-3:2018[20] (±0.015 mm).

Limitations

It is important to note that clinical OCT devices present several limitations versus laboratory-developed instruments specifically designed for lens shape measurement.[15] Firstly, clinical OCT devices are not optimised to measure soft contact lenses suspended in fluid. In contrast, both the Optimec is830 and the in-house OCT device developed by Karnowski et al.[15] were specifically optimised to obtain B-scans of soft contact lenses with sufficient contrast for processing. Secondly, the lateral range is limited to 6 mm, meaning the lens must be laterally shifted to scan its most extreme lateral ranges (>14 mm diameter). Newer clinical spectral domain OCT devices, such as the Revo NX (Optopol Technology SA),[40] produce larger ultra-high-resolution cross-sectional B-scans (ranging from 3–18 mm), meaning this limitation only applies to older clinical OCT devices like the one in this study. Moreover, due to its relevance to rigid contact lens fitting, this paper focused on measuring the BOZR of a rigid spherical contact lens. The methods presented here can also be used to measure the curvature radius of the front curve surface of a spherical contact lens if the lens is flipped. Measurement of non-spherical surfaces (e.g. multifocal lenses) is potentially possible after modifying the last step of *BOZR calculation from B-scans* to perform the corresponding optimal numerical fitting. However, the reliability of this clinical OCT device as a profilometer cannot be extrapolated from the results of this study.

In summary, this paper has demonstrated the feasibility of using a clinical OCT device (3D OCT-1000) to visually inspect the morphology (including edges) of commercial contact lenses and measure the radius of curvature of the posterior face to a precision compatible with the ISO standard. Although the clinical OCT device cannot replace a radiuscope for ISO 18369-3:2018-compliant[20] quality-control BOZR measurements, the findings of this study suggest that clinical OCT devices may play a valuable role in contact lens research and clinical practice. It is hoped that these results will encourage further studies using newer clinical OCT devices and to motivate manufacturers to develop the necessary opto-mechanical adaptors, methods, and software to take measurements like those presented here.

Acknowledgements

This research was supported by Ministerio de Ciencia, Innovación y Universidades (Grant PID2020-114311RA-I00); Gobierno de Aragón (Grant E44- 20R).

REFERENCES

1. Fercher AF, Drexler W, Hitzenberger CK, et al. Optical coherence tomography - principles and applications. Rep. Prog. Phys. 2003; 66(2): 239-303.

2. Jaffe GJ and Caprioli J. Optical coherence tomography to detect and manage retinal disease and glaucoma. Am. J. Ophthalmol. 2004; 137(1): 156-69.

3. Costa RA, Skaf M, Melo LA Jr, et al. Retinal assessment using optical coherence tomography. Prog. Retin. Eye Res. 2006; 25(3): 325–53.

4. Chen Q, Wang J, Tao A, et al. Ultrahigh-resolution measurement by optical coherence tomography of dynamic tear film changes on contact lenses. Invest. Ophthalmol. Vis. Sci. 2010; 51: 1988–1993.

5. Shen M, Cui L, Riley C, et al. Characterization of soft contact lens edge fitting using ultra-high resolution and ultra-long scan depth optical coherence tomography. Invest. Ophthalmol. Vis. Sci. 2011; 9;52(7): 4091-7.

6. Alonso-Caneiro D, Vincent SJ, Collins MJ. Morphological changes in the conjunctiva, episclera and sclera following short-term miniscleral contact lens wear in rigid lens neophytes. Cont. Lens. Anterior Eye. 2016; 39(1): 53-61.

7. Quince Z, Alonso-Caneiro D, Read SA, Collins MJ. Static compression optical coherence elastography to measure the mechanical properties of soft contact lenses. Biomed Opt Express. 2021; 2;12(4):1821-1833.

8. Ortiz S., Siedlecki D, Pérez-Merino P, et al. Corneal topography from spectral optical coherence tomography (sOCT). Biomed Opt. Express. 2011; 2(12): 3232-47.

9. Ortiz S, Pérez-Merino P, Gambra E, et al. In vivo human crystalline lens topography. Biomed. Opt. Express. 2012; 3(10): 2471-2488.

10. Sun M, Birkenfeld J, de Castro A, et al. OCT 3D surface topography of isolated human crystalline lenses. J. Biomed. Opt. Express. 2014; 5: 3547-3561.

11. Pérez-Merino P, Velasco-Ocana M, Martinez-Enriquez E, et al. OCT-based crystalline lens topography in accommodating eyes. J. Biomed. Opt. Express. 2015; 6: 5039-5054.

12. Huang X, Anderson T, Dubra A. Retinal magnification factors at the fixation locus derived from schematic eyes with four individualized surfaces. J. Biomed Opt. Express. 2022; 8;13(7): 3786-3808.

13. Huang Y, Zhang K, Kang JU, et al. Noncontact common-path Fourier domain optical coherence tomography method for *in vitro* intraocular lens power measurement. J. Biomed. Opt. 2011; 16(12): 126005.

14. Wu Q, Wang X, Liu L et al. Inspection of intraocular lens with Dual-Side View Optical Coherence Tomography. IEEE Photonics Journal. 2021;13(3): 1-10.

15. Karnowski K, Grulkowski I, Mohan N, et al. Quantitative optical inspection of contact lenses immersed in wet cell using swept source OCT. Optics Letters. 2014; 39(16): 4727-4730.

16. Verrier I, Veillas C, and Lépine T. Low coherence interferometry for central thickness measurement of rigid and soft contact lenses. Opt. Express. 2009;17(11): 9157-70.

17. Shen M, Wang MR, Wang J, et al. Entire contact lens imaged in vivo and *in vitro* with spectral domain optical coherence tomography. Eye Contact Lens. 36(2): 73-6 (2010).

18. Kaluzny BJ, Stachura J, Mlyniuk P, et al. Change in the geometry of positive- and negative-powered soft contact lenses during wear. PLoS One. 2020; 15(11): e0242095.

19. Mlyniuk P, Stachura J, Jiménez-Villar A, et al. Changes in the geometry of modern daily disposable soft contact lenses during wear. Sci. Rep. 2021; 11(1): 12460.

20. Ophthalmic Optics. Contact lenses. Part 3: Measurement Methods. ISO-18369-3 I (2018).

21. Optimec Systems (England). Optimec is830. [cited 2023 March 29] Available from: https://www.optimecsystems.com/solutions/optimec-is830/.

22. Coldrick BJ, Richards C, Sugden K, et al. Developments in contact lens measurement: A comparative study of industry standard geometric inspection and optical coherence tomography. Cont. Lens. Anterior Eye. 2016;39(4): 270-6.

23. Tankam P, Won J, Canavesi C, et al. Optical Assessment of Soft Contact Lens Edge-Thickness. Optom. Vis. Sci. 2016; 93(8): 987-96.

24. La Hood D. Edge shape and comfort of rigid lenses. Am. J. Optom. Physiol Opt. 1988; 65(8): 613-8.

25. Kittler J and Illingworth J. Minimum Error Thresholding. Pattern Recognition. 1986; 19(1): 41-47.

26. Ares J and Arines J. Influence of thresholding on centroid statistics: full analytical description. Appl. Opt. 2004; 1;43(31): 5796-805.

27. Sun Microsystems Inc. and Stanford University. Direct least-squares fitting of algebraic surfaces. Computer Graphics. 1987; 21: 145-152.

28. Ophthalmic optics. Contact lenses. Part 2: Tolerances. ISO-18369-2 I (2018).

29. Shen M, Wang MR, Wang J, et al. Entire contact lens imaged in vivo and *in vitro* with spectral domain optical coherence tomography. Eye Contact Lens. 2010; 36(2): 73-6.

30. Davidson BR, Barton JK. Application of optical coherence tomography to automated contact lens metrology. J. Biomed. Opt. Express. 2010; 15(1): 016009.

31. Wolffsohn JS, Drew T, Dhallu S, et al. Impact of soft contact lens edge design and midperipheral lens shape on the epithelium and its indentation with lens mobility. Invest. Ophthalmol. Vis. Sci. 2013; 11;54(9): 6190-7.

32. Sorbara L, Simpson TL, Maram J, et al. Optical edge effects create conjunctival indentation thickness artefacts. Ophthalmic Physiol Opt. 2015; 35(3): 283-92.

33. A Turhan SA, Toker E. Optical coherence tomography to evaluate the interaction of different edge designs of four different silicone hydrogel lenses with the ocular surface. Clin Ophthalmol. 2015; 25(9): 935-42.

34. B Maïssa C, Guillon M, Garofalo RJ. Contact lens-induced circumlimbal staining in silicone hydrogel contact lenses worn on a daily wear basis. Eye Contact Lens. 2012; 38(1):16-26.

35. C Jandl A, Ruland T, Schwarz D, Wolffsohn JS, Pult H, Bandlitz S. Clinical significance of contact lens related changes of ocular surface tissue observed on optical coherence images. Cont Lens Anterior Eye. 2021; 44(6):101388.

36. Tankam P, Won J, Canavesi C, et al. Optical Assessment of Soft Contact Lens Edge-Thickness. Optom. Vis. Sci. 2016; 93(8): 987-96.

37. Westphal W, Rollins AM, Radhakrishnan S, et al. Correction of geometric and refractive image distortions in optical coherence tomography applying Fermat's principle. Opt. Express 2002;10(9): 397-404.

38. Borja D, Siedlecki D, de Castro A, et al. Distortions of the posterior surface in optical coherence tomography images of the isolated crystalline lens: effect of the lens index gradient. J. Biomed Opt. Express. 2010;1(5): 1331-1340.

39. Podoleanu A, Charalambous I, Please L, et al. Correction of distortions in optical coherence tomography imaging of the eye. Phys. Med. Biol. 2004; 7;49(7): 1277-94.

40. OptoPol Technology (Poland). Revo NX130 [cited 2023 March 29] Available from: https://www.optopol.com/products/revo-nx-130

APPENDIX

Appendix A – Measurement data

The table below provides the mean and standard deviation of the different measurements taken in this study.

Table A. BOZR values obtained by optical radiuscope and by OCT image processing, taken in different sessions and by different operators.

CLs	**Procedures, sessions and operators**			
Nominal base curve [mm] **Nominal_BOZR**	Radiuscope base curve (mm) **Radiuscope BOZR** Mean ±SD	OCT base curve (mm) **BOZR_O1S1** Mean ±SD	OCT base curve (mm) **BOZR_O1S2** Mean ±SD	OCT base curve (mm) **BOZR_O2S1** Mean ±SD
7.30	7.26 ± 0.01	7.27 ± 0.03	7.26 ± 0.01	7.31 ± 0.06
7.40	7.39 ± 0.01	7.46 ± 0.01	7.42 ± 0.05	7.33 ± 0.02
7.50	7.48 ± 0.01	7.57 ± 0.04	7.48 ± 0.04	7.51 ± 0.09
7.55	7.55 ± 0.01	7.56 ± 0.01	7.56 ± 0.07	7.59 ± 0.04
7.60	7.57 ± 0.01	7.66 ± 0.09	7.57 ± 0.03	7.62 ± 0.12
7.65	7.61 ± 0.01	7.65 ± 0.03	7.67 ± 0.02	7.61 ± 0.06
7.70	7.69 ± 0.01	7.66 ± 0.10	7.67 ± 0.03	7.71 ± 0.08
7.75	7.78 ± 0.00	7.73 ± 0.05	7.72 ± 0.07	7.71 ± 0.04
7.80	7.81 ± 0.01	7.78 ± 0.01	7.77 ± 0.01	7.82 ± 0.05
7.85	7.83 ± 0.01	7.81 ± 0.02	7.84 ± 0.03	7.88 ± 0.11
7.90	7.88 ± 0.01	7.86 ± 0.01	7.88 ± 0.01	7.85 ± 0.03
7.95	7.93 ± 0.01	7.90 ± 0.04	7.90 ± 0.01	7.87 ± 0.03
8.00	7.99 ± 0.01	7.94 ± 0.05	7.97 ± 0.01	8.03 ± 0.10
8.05	8.03 ± 0.00	8.03 ± 0.03	8.07 ± 0.08	8.06 ± 0.11
8.10	8.13 ± 0.00	8.11 ± 0.13	8.07 ± 0.01	8.14 ± 0.11
8.15	8.17 ± 0.00	8.10 ± 0.05	8.22 ± 0.01	8.10 ± 0.01
8.30	8.29 ± 0.01	8.20 ± 0.03	8.29 ± 0.03	8.25 ± 0.06
8.40	8.35 ± 0.01	8.30 ± 0.03	8.35 ± 0.03	8.32 ± 0.10

CLs: contact lenses; O1s1: Operator1-Session1; O1s2: Operator1-Session2; O2s1: Operator2-Session1; SD: standard deviation.

Table 1. Technical specifications of the contact lens sample used in edge assessment.

	Brand	Manufacturer	Lens type	Material / RI	Power (D)	BOZR (mm) / S_depth (µm)	TD (mm)	DK
a)	Alexa 20 Aspherica	Tiedra	Spherical RL	Pasifocon A / 1.4373	+3.50 Sph	8.15/-	9.60	16
b)	Torica GP Polycon II	Lenticon	Back Torical SL	Silafocon A / 1.473	-3.00 Sph	7.30_7.80/-	9.60	10
c)	ICD™ Mini	Lenticon	Spherical SRGPL	Paflufocon D / 1.442	-7.00 Sph	-/3700	14.50	100
d)	ICD™	Lenticon	Spherical SRGPL	Paflufocon D / 1.442	-2.00 Sph	-/4200	16.50	100

	Brand	Manufacturer	Lens type	Material / RI	Power (D)	Axis (Degree)	BCR (mm)	TD (mm)	% Water
e)	Gold Medalist™ Toric	Bausch & Lomb	Torical SCL	Hefilcon C / 1.410	-2.00 Sph -1.75 Cyl	180	8.60	14.20	57
f)	Acuvue® 1-Day	Johnson & Jonhson	Spherical SCL	Etafilcon A / 1.405	-4.50 Sph	-	8.50	14.20	58
g)	Air Optix™ for astigmatism	CIBA Vision GmbH (Alcon)	Torical SCL	Lotrafilcon B / 1.421	-2.00 Sph -2.25 Cyl	70	8.70	14.50	33
h)	Toric 55	Aspect Vision Care	Torical SCL	Methafilcon A / 1.420	-2.00 Sph -1.25 Cyl	180	8.70	14.40	55

RI: refraction index; D: Dioptre; BOZR: back optic zone radius; BCR: base curve radius; S_depth: sagittal depth; TD: total diameter; Dk: contact lens oxygen permeability in barrers; RL: rigid lens; SRGPL: scleral rigid gas-permeable lens; SCL: soft contact lens.

Table 2. Variability, intra-class correlation coefficient and Student's *t*-test results.

Dataset	VC	Sd_Diff(mm)	max_Diff Absolute Error (mm)
O1s1	0.75%	0.0590	0.110
O1s2	0.50%	0.0390	0.104
O2s1	0.75%	0.0590	0.130
Sim noise-free	*0.016%*	*0.0013*	*0.006*
Sim minimum spatial noise	*0.23%*	*0.0180*	*0.065*

Comparison	Student's *t*-test p-value	CCI
BOZR_O1s1 vs BOZR_O1s2	0.666	0.991 (p < 0.001)
BOZR_O1s2 vs BOZR_O2s1	0.997	0.984 (p < 0.001)
BOZR_O1s1 vs BOZR_O2s1	0.660	0.986 (p < 0.001)
BOZR_O1s1 vs radiuscope BOZR	0.661	0.992 (p < 0.001)
BOZR_O2s1 vs radiuscope BOZR	0.996	0.991 (p < 0.001)

VC: variation coefficient; Sd_Diff: standard deviation of the difference; max_Diff: absolute value of the maximum error of the difference; CCI: intra-class correlation coefficient. O1s1: Operator1-Session1; O1s2: Operator1-Session2; O2s1: Operator2-Session1.

[Figure legends]

Figure 1. Contact lens adaptor placed in front of a 3D OCT-1000 with a tilted flat mirror.

Figure 2. Image processing and OCT B-scan analysis flow-chart.

Figure 3. Original *in vitro* cropped B-scans of different lens edges of several commercial rigid gas-permeable contact lenses and soft contact lenses. (a) Spherical RGP ("Alexa 20 Asphérica"; Tiedra), (b) torical RGP ("Torica GP Polycon II"; Lenticon), (c) rigid scleral lens ("ICD™), (d) rigid scleral lens ("ICD™; Paragon), (e) torical SCL ("Gold Medalist™ Toric"; Bausch & Lomb), (f) spherical SCL ("Acuvue® 1-Day"; Johnson & Jonhson), (g) torical SCL ("Air Optix™ for astigmatism"; CIBA Vision, Alcon) and (h) torical SCL ("Toric 55"; Aspect Vision Care). The scale shown in Figure 3(f) is the same for all sub-images. A torical marking is surrounded by a white dashed circle in Figure 3(b).

Figure 4: (a) Bland–Altman plot of intra-session (BOZR Operator1-Session1 and BOZR Operator1-Session2) differences, and (b) intra-operator (BOZR Operator1-Session1 and BOZR Operator2-Session1) differences.

Figure 5: Bland–Altman plots for BOZR measurement differences between radiuscope measurements and two different operators. (a) Differences between radiuscope BOZR values and the measurements taken by Operator1-Session1 (BOZR Operator1-Session1). (b) Differences between radiuscope BOZR values and the measurements taken by Operator2 (BOZR Operator2-Session1).

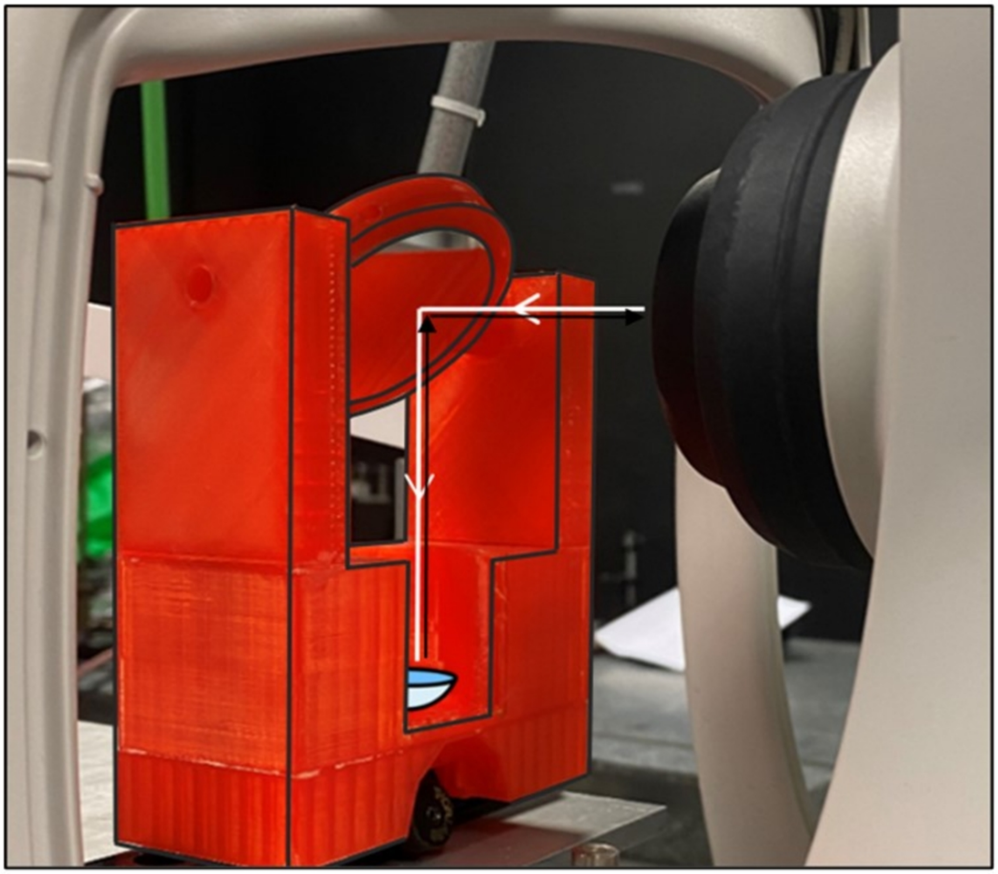

Figure 1. Contact lenses adaptor emplaced in front of 3-D OCT-1000 with a tilted flat-mirror.

317x279mm (400 x 400 DPI)

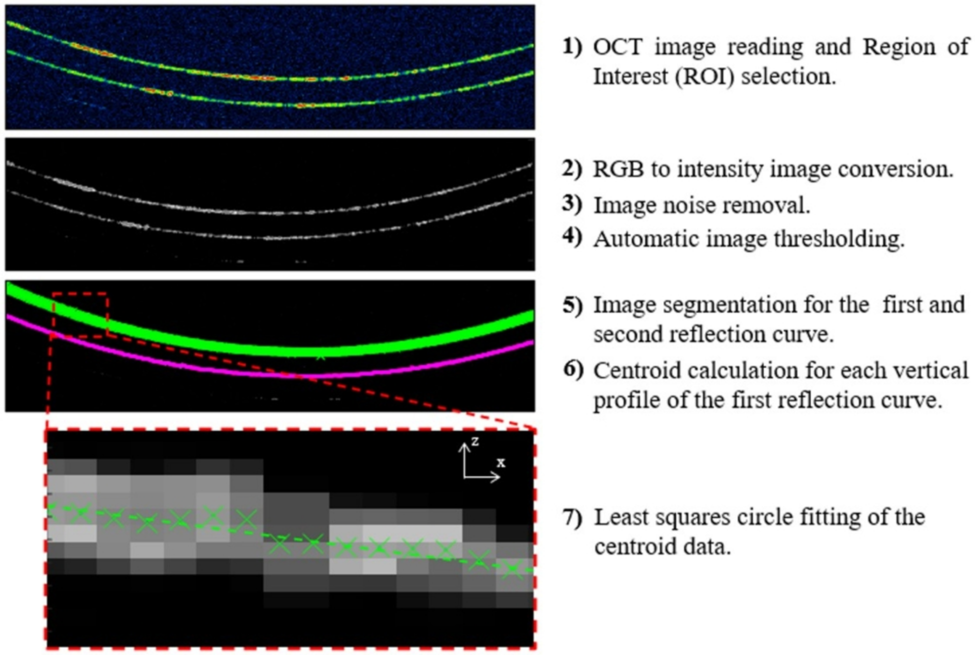

Figure 2. Flow chart of image processing and analysis of the B-scan OCT image.

381x255mm (400 x 400 DPI)

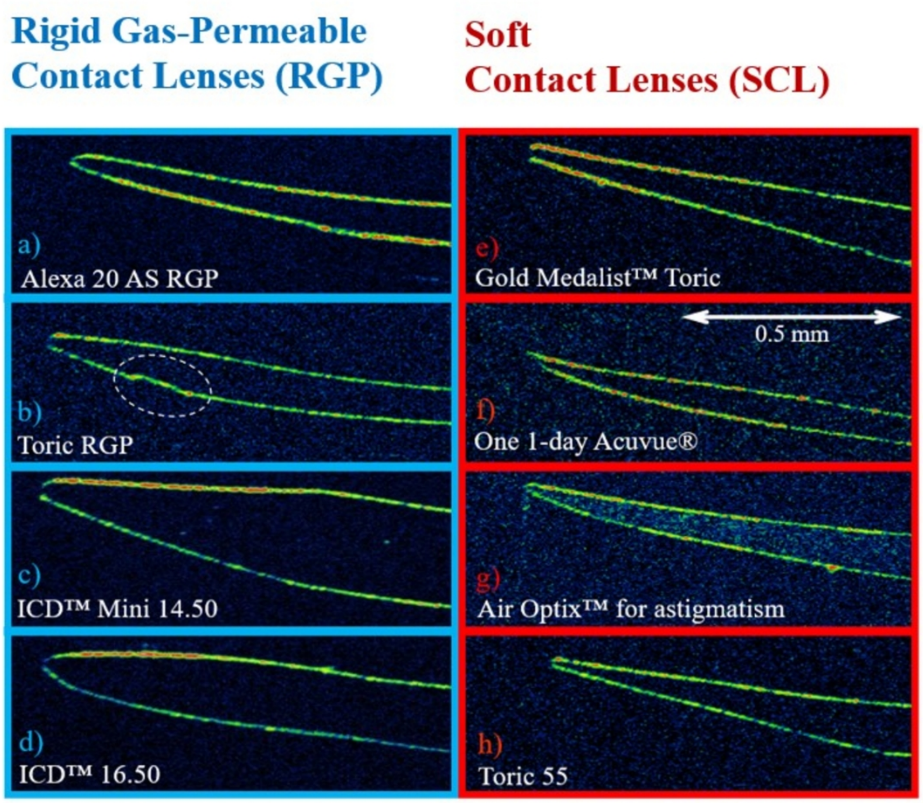

Figure 3. Original in-vitro cropped B-scan images of different lens edges for some commercial rigid gas-permeable contact lenses and soft contact lenses. (a) Spherical RGP "Alexa 20 Aspherica" (Tiedra), (b) toric RGP "Torica GP Polycon II" (Lenticon), (c) rigid scleral lens "ICD™, (d) rigid Scleral lens "ICD™ (Paragon), (e) toric SCL "Gold Medalist™ Toric" (Bausch & Lomb), (f) spheric SCL "Acuvue® 1-Day" (Johnson & Jonhson), (g) toric SCL "Air Optix™ for astigmatism" (CIBA Vision, Alcon) and (h) Toric SCL "Toric 55" (Aspect Vision Care). The scale size shown at subFigure (f) is the same for all sub-images. A toric marking is surrounded with a white dashed circle at subFigure (b).

381x314mm (400 x 400 DPI)

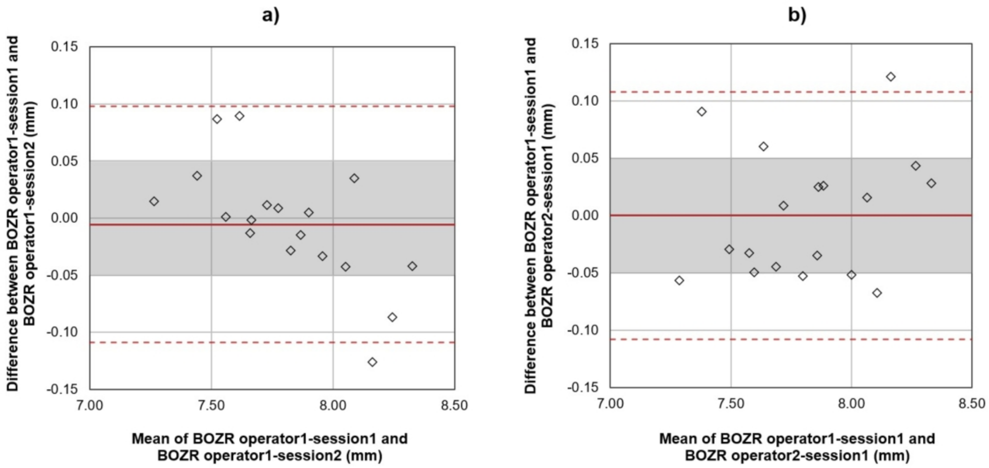

Figure 4: (a) Bland-Altman plot of intra-session (BOZR operator1-session1 and BOZR operator1-session2) and (b) intra-operator (BOZR operator1-session1 and BOZR operator2-session1) differences.

381x189mm (399 x 399 DPI)

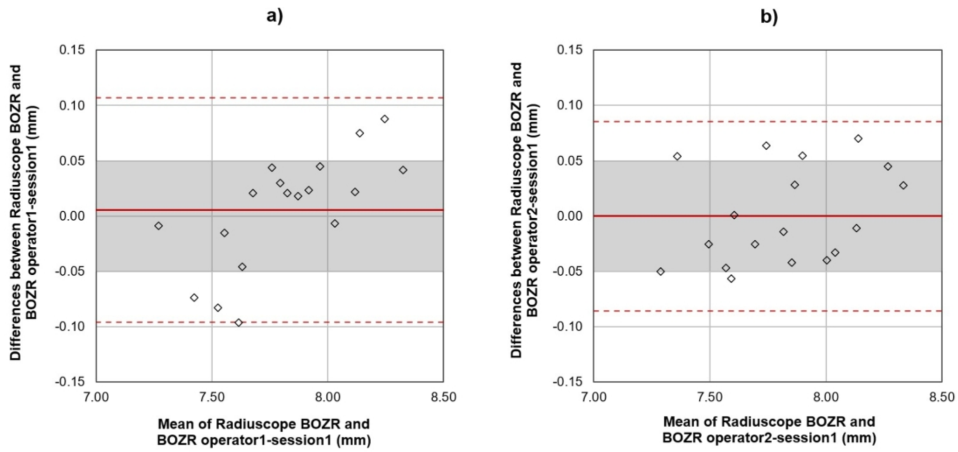

Figure 5: Bland-Altman plots for BOZR measurement differences between Radiuscope measurements and two different operators. (a) Differences between Radiuscope BOZR values and the measurements taken by operator1-session1 (BOZR operator1-session1). (b) Differences between Radiuscope BOZR values and the measurements taken by operator 2 (BOZR operator2-session1).

382x175mm (398 x 398 DPI)